ISSN 1070-3284, Russian Journal of Coordination Chemistry, 2021, Vol. 47, No. 4, pp. 244–252. © Pleiades Publishing, Ltd., 2021.
Russian Text © The Author(s), 2021, published in Koordinatsionnaya Khimiya, 2021, Vol. 47, No. 4, pp. 208–217.

Complexes of Lanthanide (Dy, Er, Yb) Thiocyanates with Tetramethylphenanthroline. Synthesis, Thermolysis, and SMM Properties

S. P. Petrosyants[a], *, K. A. Babeshkin[a], **, A. B. Ilyukhin[a], E. V. Belova[a, b], and N. N. Efimov[a]

[a] *Kurnakov Institute of General and Inorganic Chemistry, Russian Academy of Sciences, Moscow, Russia*

[b] *Moscow State University, Moscow, Russia*

**e-mail: petros@igic.ras.ru*

***e-mail: bkonstantan@yandex.ru*

Received August 31, 2020; revised October 12, 2020; accepted October 21, 2020

Abstract—The mononuclear neutral complexes $[Ln(Me_4Phen)_2(H_2O)(NCS)_3]\cdot Me_4Phen\cdot 0.75EtOH$ (Ln = Dy, Er, Yb) were prepared for the first time by the reaction of $[Ln(H_2O)_5(NCS)_3]\cdot H_2O$ (Ln = Dy, Er, Yb) with 3,4,7,8-tetramethyl-1,10-phenanthroline (Me_4Phen) in ethanol. The products were identified by elemental analysis and powder X-ray diffraction. A thermoanalytical study of the products revealed the transfer of the outer-sphere Me_4Phen ligand to the first coordination sphere. The obtained compounds were found to behave as single-molecule magnets.

Keywords: Dy, Er, and Yb thiocyanates, Me_4Phen, magnetic properties, single-molecule magnets

DOI: 10.1134/S1070328421040060

INTRODUCTION

The interest in heteroleptic lanthanide thiocyanate complexes containing polydentate N-donor ligands (Bipy = 2,2'-bipyridine, Phen = 1,10-phenanthroline, etc.) is due to their use for extraction, for the design of new types of sensors [1], and as drug components for the treatment of breast cancer [2]. Study of the photophysical properties has shown good prospects for the use of various nitrogen-containing ligands for sensitization of Ln3+ luminescence in these compounds [3–10]. The electronic structure of the unfilled 4f orbitals accounts for the potential use of Ln3+ in the targeted design of systems with diverse magnetic properties [11, 12].

Among lanthanides, dysprosium is best studied as the magnetic center for single-molecule magnets (SMMs); the efficiency of Dy is confirmed by the latest publications of Prof. Lifield's group [13]. In recent years, attention of researchers has been also attracted by compounds of other Kramer ions (the ions with odd numbers of electrons) of heavy lanthanides, in particular, Er and Yb, which exhibit slow relaxation. It is noteworthy that the comparative studies of SMMs based on heteroleptic Er and Yb complexes are now at the stage of accumulation and systematization, unlike the extensive body of information existing for dysprosium. The increased attention to the three mentioned lanthanides is caused by the ground state bistability. This is a major factor responsible for the SMM behavior of compositionally and structurally diverse compounds of these lanthanides [14–25].

The slow magnetic relaxation of the complex directly depends on the coordination environment of the magnetic center, i.e., the nature of ligands, the type of polyhedron, and the relative positions of donor sites in the polyhedron, especially for SMMs containing no Dy. We showed that the energy barriers for magnetization reversal (ΔE) for a series of mononuclear Bipy and Phen complexes of dysprosium thiocyanates directly depend on the structural features of the compounds [26], which was later confirmed for analogous series of Er^{3+} and Yb^{3+} [27].

This study is directed towards the expansion of our views on the targeted synthesis of mononuclear 4*f* SMMs and towards further investigation of the dependence of magnetic properties of lanthanide thiocyanate compounds on their coordination environment (CE). In order to expand the range of studied compounds of Kramer heavy lanthanide ions, we prepared for the first time Dy^{3+}, Er^{3+}, and Yb^{3+} thiocyanate complexes with 3,4,7,8-tetramethyl-1,10-phenanthroline (Me_4Phen). All of the isolated compounds were identified using elemental analysis and powder X-ray diffraction.

EXPERIMENTAL

Commercial $[Ln(H_2O)_5(NCS)_3]\cdot H_2O$ (Ln = Dy [26], Er, Yb [27], Me_4Phen (99%, Aldrich), and ethanol (C_2H_5OH) as the solvent were used as received. All operations were carried out in air.

Synthesis of $[Ln(Me_4Phen)_2(H_2O)(NCS)_3]\cdot Me_4Phen\cdot 0.75EtOH$ (Ln = Dy (**I**), Er (**II**), Yb (**III**). A solution of $[Ln(H_2O)_5(NCS)_3]\cdot H_2O$ (0.2 mmol in 15 mL of C_2H_5OH) was added to a solution of Me_4Phen (0.6 mmol) in C_2H_5OH (10 mL), the mixture was stirred for ~30 min and left at room temperature for complete crystallization. After 3 days, the solid phase was separated on a paper filter, washed with ethanol, and dried at room temperature.

The yield of **I** was 0.16 g (72% based on Dy).

For $C_{52.5}H_{54.5}N_9O_{1.75}S_3Dy$ (M = 1098.25)

Anal. calcd., %	C, 57.41	H, 5.00	N, 11.48	S, 8.76
Found, %	C, 57.63	H, 4.57	N, 11.76	S, 8.82

The yield of **II** was 0.17 g (77% based on Er).

For $C_{52.5}H_{54.5}N_9O_{1.75}S_3Er$ (M = 1103.01)

Anal. calcd., %	C, 57.17	H, 4.98	N, 11.43	S, 8.72
Found, %	C, 57.50	H, 4.54	N, 11.95	S, 8.93

The yield of **III** was 0.14 g (64% based on Yb).

For $C_{52.5}H_{54.5}N_9O_{1.75}S_3Yb$ (M = 1108.79)

Anal. calcd., %	C, 56.87	H, 4.95	N, 11.36	S, 8.68
Found, %	C, 56.72	H, 4.54	N, 11.80	S, 8.93

Elemental analysis was performed on a EUROEA 3000 CHN analyzer by standard procedures. Powder X-ray diffraction analysis was carried out on a Bruker D8 Advance diffractometer (CuK_α, λ = 1.5419 Å, Ni filter, LYNXEYE detector, reflection geometry) at the Center for Collective Use, Kurnakov Institute of General and Inorganic Chemistry, Russian Academy of Sciences. The full-profile Rietveld refinement of structures **I**–**III** was done using the TOPAS program [28]. The atomic coordinates were derived from X-ray diffraction data for complex $[Y(Me_4Phen)_2(H_2O)(NCS)_3]\cdot Me_4Phen\cdot 0.75EtOH$ (**IV**) isostructural to **I**–**III** [29]. In the structure of **IV**, one NCS ligand is disordered over two positions; the occupancy of the position of the EtOH solvate molecule is 0.75. In the refinement of the structures of **I**–**III**, the coordinates of all atoms, except for Ln, were fixed, the occupancy of the EtOH solvate molecule was fixed (0.75), and the occupancies of the disordered NCS ligand were refined. In the final refinement cycles, all atomic coordinates and occupancies were also fixed.

The thermal stability of the obtained compounds was studied by differential scanning calorimetry (DSC) and thermogravimetry (TG) using NETZSCH DSC 204 F1 and NETZSCH TG 209 F1 instruments, respectively. The argon flow rates were 40 mL/min for DSC and 30 mL/min for TG. The DSC was performed in a DSC 204 F1 NETZSCH calorimeter in the temperature range of 35–500°C at a heating rate of 10°C/min. The mass loss during thermolysis in the 35–500°C temperature range was determined on a TG 209 F1 NETZSCH thermobalance at a heating rate of 10°/min. The effluent gas was analyzed using a QMS 403C mass-spectrometric attachment conjugated with the thermobalance. Before measuring the TGA curves, the furnace was evacuated and filled with argon to remove traces of air. The results of thermal analysis were processed according to the ISO 11357-1, ISO 11357-2, ISO 11358, and ASTM E 1269-95 standards using the NETZSCH Proteus Thermal Analysis package.

The magnetic behavior of complexes **I**–**III** was investigated by static and dynamic magnetic susceptibility methods on a PPMS-9 magnetometer (QuantumDesign) in the 2–300 K temperature range in 0–5000 Oe static magnetic fields. The dynamic magnetic susceptibility was studied using 5, 3, and 1 Oe alternating magnetic fields for 10–100, 100–1000, and 10–10000 Hz frequency ranges of the field, respectively. These measurement conditions made it possible to avoid sample warming-up at low temperatures (can take place at large amplitude and modulation frequency) and to attain the best signal-to-noise ratio. All magnetic measurements were carried out for milled polycrystalline samples sealed in polyethylene bags and frozen in mineral oil to prevent the magnetic field-induced orientation of crystallites [30]. The paramagnetic component of the magnetic susceptibility (χ) was determined taking into account diamagnetic contributions of the sample, mineral oil, and sample holder.

RESULTS AND DISCUSSION

Complexes **I**–**III** were synthesized in ethanol, with the ligand to metal ratio being 3 : 1. This is the optimal composition of reactants, as shown for the synthesis of similar Y, Eu, and Tb complexes [29]. Under these conditions, complexes **I**–**III** were obtained in >60% yields. The elemental analysis data were in good agreement with the theoretical composition of the complexes. Powder X-ray diffraction analysis confirmed that the products were pure and isostructural to the yttrium analogue $[Y(Me_4Phen)_2(H_2O)(NCS)_3]\cdot Me_4Phen\cdot 0.75EtOH$. Since we did not succeed in growing single crystals suitable for single crystal X-ray diffraction, the structures of $[Ln(Me_4Phen)_2(H_2O)(NCS)_3]\cdot Me_4Phen\cdot 0.75EtOH$ (Ln = Dy, Er, Yb) were refined using the powder X-ray diffraction data (Table 1, Figs. S1–S3).

The Ln coordination number in the molecular complex $[Ln(Me_4Phen)_2(H_2O)(NCS)_3]$ (Fig. 1) is

Table 1. Key structural data and structure refinement details for **I**–**III**

Parameter	Value		
	I	**II**	**III**
T, K	296	296	296
System	Monoclinic	Monoclinic	Monoclinic
Space group	$P2_1/n$	$P2_1/n$	$P2_1/n$
a, Å	13.0480(16)	13.0289(8)	13.0087(10)
b, Å	16.4683(18)	16.4646(10)	16.4611(13)
c, Å	24.144(2)	24.1272(14)	24.1151(15)
β, deg	100.263(6)	100.229(5)	100.185(5)
V, Å^3	5105(1)	5093.4(5)	5082.6(6)
Z	4	4	4
Range of 2θ, deg	5–50	4–50	4–50
Step of 2θ, deg	0.02	0.02	0.02
R_{exp}	2.18	2.44	3.22
Rwp	3.72	7.22	6.35
Rp	2.86	5.29	4.95
GOOF	1.71	2.96	1.97
R_{Bragg}	1.93	3.51	3.27

eight, the coordination polyhedron is a square antiprism, and the coordination unit is $LnON_7$. The bases of the square antiprism are composed of the $N_1N_4N_5O_1$ and $N_2N_3N_6N_7$ atoms, where N_1 is the nitrogen atom of the NCS^- group disordered over two positions; N_2 and N_3 belong to other NCS^- groups; N_4, N_5 and N_6, N_7 belong in pairs to different Me_4Phen molecules; and O_1 is oxygen of the coordinated water molecule (Fig. S4). The distance between the bases of the square antiprism is 2.8147 Å, and the angle between the base planes is close to 1.1°. The average deviations of atoms from the mean planes of the two square bases of the antiprism are 0.1098 Å for $N_1N_4N_5O_1$ and 0.0186 Å for $N_2N_3N_6N_7$, respectively. The distances between the Ln^{3+} ion and coordination polyhedron atoms vary from 2.3610 Å for Ln–O to 2.5653 Å for Ln–N_7. The uncoordinated Me_4Phen molecule is involved in the stacking interaction with one Me_4Phen ligand. The shortest Ln...Ln distances are 9.77, 9.75, and 9.70 Å for Dy, Er, and Yb, respectively.

In the solid-phase thermolysis of compounds **I**–**III**, the removal of C_2H_5OH solvate molecules is detected in the 25–100°C temperature range (the mass spectrum showed $[OH]^+$, $[C_2H_5]^+$, and $[C_2H_5OH]^+$ ions with *m*/*z* 17, 29, and 46, respectively): this process is accompanied by heat absorption (Fig. 2a) and by decrease in the sample mass (Fig. 2b). The experimental mass loss (1.03%) proves to be lower than the expected one (4.0%), since the solvate molecules are partly removed during evacuation of the furnace.

On further heating to 150°C, removal of the coordinated water molecule starts and continues up to 200°C (the mass spectrum exhibited $[H_2O]^+$ and $[OH]^+$ ions with *m*/*z* of 18 and 17, respectively); this is accompanied by heat absorption (Fig. 2a) and a slight mass loss (Fig. 2b). The experimental mass loss of

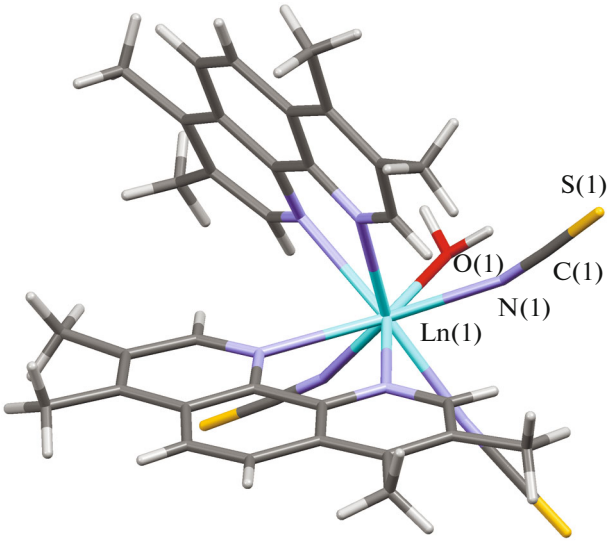

Fig. 1. Structure of the inner sphere of the complex $[Ln(Me_4Phen)_2(H_2O)(NCS)_3]$, where Ln(1) is Dy (**I**), Er (**II**), or Yb (**III**).

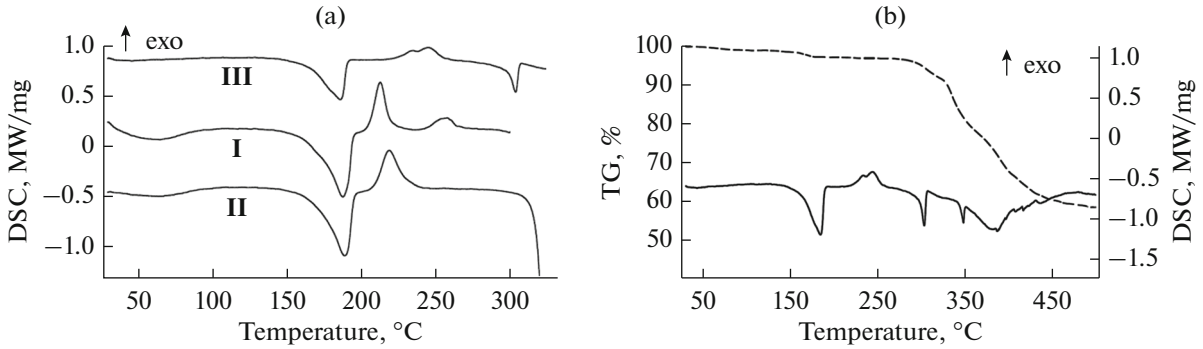

Fig. 2. (a) DSC curves of complexes **I**–**III** in the 25–300°C range; (b) TG (dashed line) and DSC curves (continuous line) of complex **III** (Ln = Yb).

1.8% is consistent with the expected one (2.1%) within the experimental error.

After water has been removed from the inner coordination sphere, all three complexes exhibit exothermic effects not accompanied by a loss of mass. These effects could be associated with a solid-phase chemical reaction, or ordering of an amorphous or metastable structure inherited after removal of the solvent, or both. Recrystallization/crystallization of an amorphous material is a spontaneous process and necessarily takes place if the relaxation time at the given temperature is comparable with the time of experiment. Immediately after removal of the solvent, the compound is more often amorphous to X-rays, but on further heating and maintaining in the temperature range in which the exotherm appears in the DSC curve, the X-ray diffraction pattern exhibits reflections that do not belong to the precursor. Apparently, these effects are associated with the formation of a new crystal structure. Presumably, Me_4Phen enters the inner coordination sphere of the dehydration product. A similar phenomenon was observed previously for isostructural Y, Eu, and Tb complexes [29]. For those complexes, the insertion of the outer-sphere Me_4Phen group into the inner sphere was also confirmed by change in the powder X-ray diffraction pattern after TG. Unlike Y, Eu, or Tb, in the case of complexes **I** (Dy) and **III** (Yb), a superposition of several exotherms rather than a single exotherm appears. In all probability, this is due to the fact that crystallization and formation of ligand–metal bonds is not a one-step process.

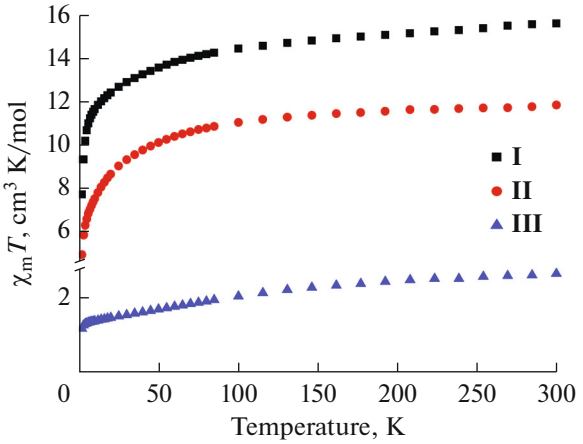

Fig. 3. Temperature dependences $\chi_m T(T)$ for compounds **I**–**III** in a 5000 Oe static magnetic field.

The magnetic behavior of all complexes was investigated in the range of 2–300 K in a 5000 Oe external magnetic field (Fig. 3). Since the shortest Ln...Ln distances in compounds **I**–**III** are more than 9.70 Å, the lanthanide ions can be considered to be isolated magnetic centers. This is confirmed by both the patterns of $\chi_m T$ dependences characteristic of complexes of the corresponding lanthanides and the proximity of $\chi_m T$ values observed at 300 K to theoretical $\chi_m T$ values of isolated Ln^{3+} ions (Table 2). In the case of complex **I**, the $\chi_m T$ values decrease insignificantly as the temperature decreases to 60 K, while on further cooling, the decrease is more pronounced; a sharp drop occurs at 6 K and the minimum value is observed at 2 K. The dependence for complex **II** is similar to that of **I**, but the decline at low temperatures is more gradual. In the case of complex **III**, the behavior is typical of Yb complexes: $\chi_m T$ uniformly decreases on cooling down to 4 K, which is followed by faster approach to the minimum value.

Complexes **I**–**III** synthesized in this work contain Kramer ions able to exhibit slow magnetic relaxation. In order to study the magnetic dynamics of the complexes, we measured the magnetic susceptibility in an alternating magnetic field. For all of the compounds, in a zero magnetic field, the dependences of the imaginary part of the dynamic magnetic susceptibility ($\chi''(\nu)$) do not show significant signals. This may be due to the quantum tunneling of magnetization (QTM) [32], which is manifested as a considerable decrease in the relaxation time of magnetization. For

Table 2. Magnetic susceptibility of the complexes in a 5000 Oe static magnetic field

Compound	$\chi_m T$ (300 K)	$\chi_m T$ (theor.) [31]	$\chi_m T$ (2 K)
	cm^3 K/mol		
I	15.59	14.17	7.71
II	11.83	11.48	4.93
III	2.65	2.57	1.18

suppressing QTM, the dynamic magnetic susceptibility measurements were carried out in static magnetic fields of different strengths (0–5000 Oe). In non-zero external magnetic fields, slow magnetic relaxation was detected for all of the compounds. The optimal magnetic field strengths (H_{dc}), which correspond to the greatest relaxation times, are 1000 Oe for **I** and **II** and 2500 Oe for **III** (Figs. S5–S7). For better understanding of the dynamics of slow magnetic relaxation, it is necessary to evaluate the contributions of various mechanisms to the magnetization relaxation. The approximation of experimental $\chi''(\nu)$ data in the optimal field (Fig. 4) using the generalized Debye model resulted in the dependence of the relaxation time on the reciprocal temperature $\tau(1/T)$ (Fig. 5).

The relaxation parameters for the prepared compounds were determined by approximating the high-temperature regions of the dependences $\tau(1/T)$ by the Arrhenius equation $\tau_{Or} = \tau_0 \exp(\Delta E/k_B T)$, where ΔE is the height of the energy barrier for the magnetization reversal; k_B is the Boltzmann constant, τ_0 is the shortest relaxation time, T is temperature. This expression is the mathematical description of the Orbach relaxation mechanism. The following ranges of the high-temperature regions were chosen for approximation: 4.5–5.5 K for complex **I**, 2.9–3.1 K for **II**, and 5.5–6.5 K for **III**. The best agreement between the theoretical dependences and experimental data was obtained for the following sets of parameters: $\tau_0 = 1.7 \times 10^{-7}$ s, $\Delta E/k_B = 28$ K (**I**); $\tau_0 = 1.2 \times 10^{-7}$ s, $\Delta E/k_B = 15$ K (**II**); $\tau_0 = 1.7 \times 10^{-7}$ s, $\Delta E/k_B = 30$ K (**III**). The results indicate that complexes **I**–**III** behave as molecular magnets when a static external magnetic field is applied.

The plots of $\tau(1/T)$ in the semilogarithmic coordinates for compounds **I**–**III** are non-linear (Fig. 5). This indicates the presence of magnetization relaxation mechanisms other than the Orbach mechanism. The data corresponding to the full temperature ranges for each complex can be approximated only if several relaxation mechanisms are taken into account. In the case of complexes **I** and **II**, good agreement with experimental data can be achieved by using the Orbach and Raman relaxation mechanisms ($\tau_{Ram}^{-1} = C_{Ram} T^{n\_Ram}$, where C_{Ram} and n_Ram are Raman relaxation mechanism parameters) for $\tau_0 = 1.3 \times 10^{-7}$ s, $\Delta E/k_B =$ 30 K, $C_{Ram} = 75$ K^{-n_Ram} s, n_Ram = 2.56 (**I**); $\tau_0 = 3.6 \times 10^{-9}$ s, $\Delta E/k_B = 29$ K, $C_{Ram} = 2630$ K^{-n_Ram} s, n_Ram = 2.29 (**II**) (Figs. 5a, 5b). The n values in the Raman relaxation equation, close to 2, attest to the so-called phonon bottleneck effect [33]. For complex **III**, the coincidence of the theoretical curve and experimental data can be attained using the sum of the Orbach and QTM relaxation mechanisms ($\tau_{KTH}^{-1} = B$), which is indicative of incomplete suppression of the tunneling effect even in a non-zero external magnetic field (Fig. 5c). The relaxation parameters resulting from approximation of experimental data in the whole

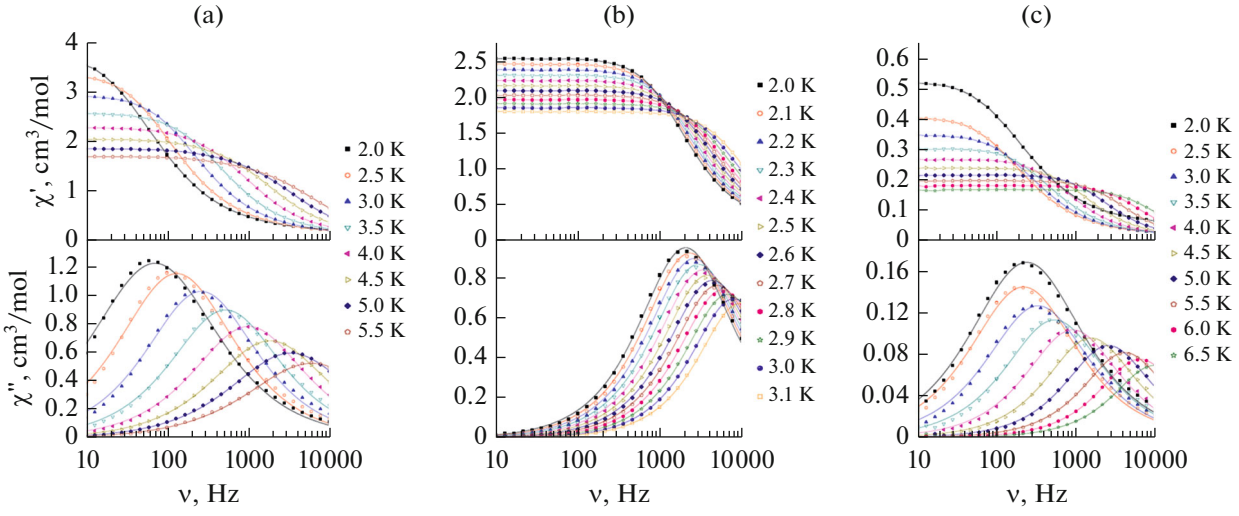

Fig. 4. Frequency dependences of the real χ' (above) and imaginary χ'' (below) components of dynamic magnetic susceptibility of complexes (a) **I**, (b) **II**, (c) **III** in 1000 (**I**, **II**) and 2500 Oe (**III**) magnetic fields in the temperature ranges of (**I**) 2–5.5, (**II**) 2–3.1, and (**III**) 2–6.5 K (the lines are visual guides (χ'), approximation by the generalized Debye model (χ'')).

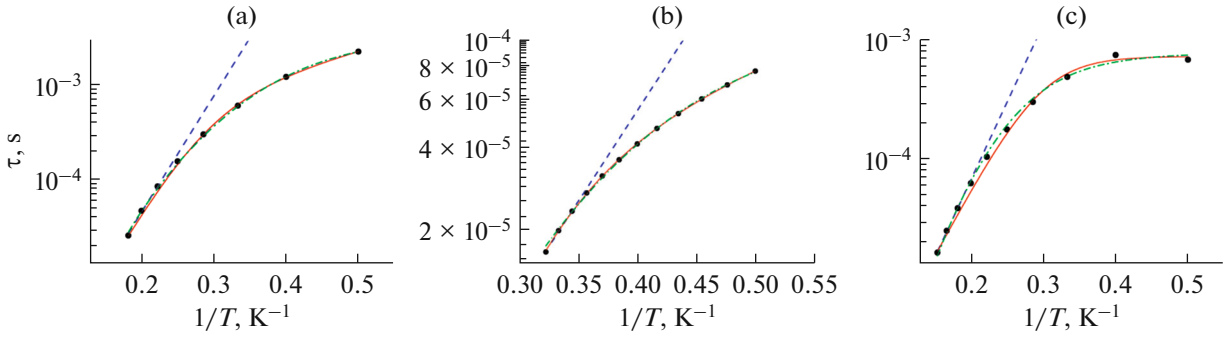

Fig. 5. Relaxation times of complexes (a) **I**, (b) **II**, (c) **III** in 1000 (**I**, **II**) and 2500 Oe (**III**) magnetic fields vs. reciprocal temperature. Dashed lines are the approximation of high-temperature regions by the Orbach mechanism; solid lines are the approximation using the sum of Orbach and Raman mechanisms (**I**, **II**) or Orbach and QTM mechanisms (**III**); and dash-and-dot lines are the approximation using the sum of Raman and QTM mechanisms.

temperature range (2–6.5 K) are as follows: $\tau_0 = 3.2 \times 10^{-7}$ s, $\Delta E/k_B = 26$ K, $B = 1410$ s. For complexes **I** and **III**, the barriers for magnetization reversal obtained for high-temperature ranges and for whole temperature regions are similar. This indicates that at temperatures above 4.5 K (for **I**) and 5.5 K (for **III**), the Orbach mechanism is the primary pathway of relaxation of the magnetization.

When considering the possible processes of relaxation of the magnetization and their combinations, one should bear in mind that the Orbach mechanism often does not contribute to relaxation. Previously, this was observed for Er and Yb thiocyanate complexes [27]. This idea is prompted by both the possibility of approximating $\tau(1/T)$ for **I**–**III** by using the sum of QTM and Raman mechanisms (Fig. 5) and a comparison of the energy barriers and τ_0 values. For compounds **I** and **III**, $\tau_0 \approx 10^{-7}$ s; meanwhile, the relaxation times characteristic of the overbarrier magnetization reversal corresponding to the Orbach mechanism should range from 10^{-10} to 10^{-12} s [34]. For complex **II**, the magnetization reversal barrier obtained by approximating the sum of the QTM and Orbach mechanisms proves to be twice as high as that obtained from high-temperature data. This also indicates that relaxation occurs by a mechanism other than Orbach mechanism [35]. However, despite the foregoing, the ΔE values derived from the Arrhenius equation can be used as rough estimates for the comparison of magnetic properties of SMMs [27].

When the sum of QTM and Raman mechanisms was used for approximation of experimental data, the following relaxation parameters were obtained: $C_{Ram} = 4.13$ K^{-n_Ram} s, n_Ram = 5.3, $B = 286$ s (**I**); $C_{Ram} = 149$ K^{-n_Ram} s, n_Ram = 5.1, $B = 7930$ s (**II**); $C_{Ram} = 1.47$ K^{-n_Ram} s, n_Ram = 5.7, $B = 1296$ s (**III**). In this case, the n_Ram values are close to one another and to n_Ram = 5. This may indicate that compounds **I**–**III** have low-lying thermally populated excited states [34]. The use of these sets of mechanisms, differing from those presented above, brings about redundant parameterization.

Dysprosium complexes are known to have the greatest ΔE values among the isostructural lanthanide complexes and all SMMs [13]; however, the barrier for magnetization reversal of complex **I** proved to be somewhat lower than ΔE of the isostructural Yb complex (**III**). For explaining the moderate barrier for magnetization reversal of **I**, we calculated the easy magnetization axis using the Magellan program (the charges of atoms were chosen as described in [33] (Fig. 6a)). It is known that for the optimal SMM behavior of a complex, it is necessary that the easy magnetization axis be close to the symmetry axis of the coordination polyhedron [36]. Apparently, the pronounced deviation of the easy magnetization axis from the symmetry axis of the square antiprism (Fig. 6b), along with the heteroleptic environment and the geometrically rigid Me_4Phen ligand, have an adverse effect on the magnetization reversal barrier.

Out of the presented Kramer ions, only Dy^{3+} has so-called oblate electron density according to the Rinehart–Long theoretical model [36]. Therefore, a linear coordination environment is optimal for retarding the magnetic relaxation in complexes of this lanthanide. In all Dy complexes presented in Table 3, the lanthanide coordination geometry considerable differs from the optimal one, which precludes achieving ΔE values close to optimal ones. Furthermore, the barrier for magnetization reversal of neutral Dy complexes is halved when the water molecules in the coordination sphere of Dy aqua thiocyanate are replaced by geometrically rigid ligands such as Bipy, Phen, or Me_4Phen. This is apparently due to the fact that the coordination polyhedron (CP) rigidity increases and, hence, steric restrictions preclude the formation of the optimal coordination geometry.

It follows from the results that ΔE for Er^{3+} ion almost does not change on going from the initial thiocyanate (double capped trigonal prism) to complex **II**

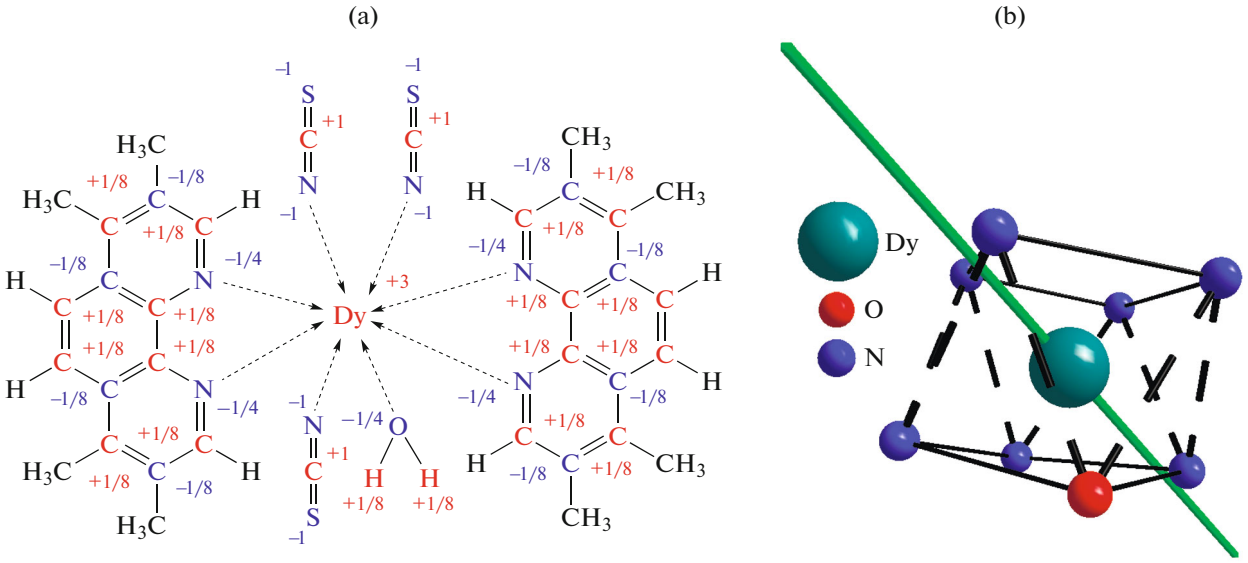

Fig. 6. (a) Theoretical charge distribution taken as the basis to calculate the easy magnetization axis; (b) direction of the easy magnetization axis relative to the square antiprismatic environment of the Dy atom.

(square antiprism). This type of behavior us unusual for erbium, as analysis of published data points to the highest sensitivity of Er^{3+} to the CE [27]. Considering the Er-based SMMs studied to date, the optimal CE of Er^{3+} is a sandwich characterized by bulky planar ligands remote from the lanthanide ion, parallel to

Table 3. Barriers for magnetization reversal ($\Delta E/k_B$, K) and optimal static magnetic fields (H_{dc}, Oe) for mononuclear neutral Dy, Er, and Yb thiocyanate complexes with bidentate N-donor ligands

Compound	C.N. (Ln)/polyhedron	$\Delta E/k_B$ Orbach/sum of mechanisms (H_{dc})	Refs.
$[Dy(H_2O)_5(NCS)_3]\cdot H_2O$	8/square antiprism or double capped trigonal prism	43 (1000)	[26]
$[Dy(Bipy)_2(H_2O)(NCS)_3]\cdot 0.5Bipy\cdot H_2O$	8/square antiprism	28 (500)	[26]
$[Dy(Phen)_2(H_2O)(NCS)_3]\cdot Phen\cdot 0.5H_2O$	8/double capped trigonal prism	27/23 (1000)	[26]
$[Dy(Me_4Phen)_2(H_2O)(NCS)_3]\cdot Me_4Phen\cdot 0.75EtOH$	8/square antiprism	28/28 – Orbach+Raman (1000)	This work
$[Er(H_2O)_5(NCS)_3]\cdot H_2O$	8/double capped trigonal prism	14 (1000)	[27]
$[Er(Me_4Phen)_2(H_2O)(NCS)_3]\cdot Me_4Phen\cdot 0.75EtOH$	8/square antiprism	15/29 – Orbach + Raman (1000)	This work
$[Yb(H_2O)_5(NCS)_3]\cdot H_2O$	8/double capped trigonal prism	50 (2500)	[27]
$[Yb(Bipy)_2(H_2O)(NCS)_3]\cdot 0.5Bipy\cdot H_2O$	8/square antiprism	47 (1000)	[27]
$[Yb(Phen)_2(H_2O)(NCS)_3]\cdot Phen\cdot 0.5H_2O$	8/double capped trigonal prism	22 (1000)	[27]
$[Yb(Me_4Phen)_2(H_2O)(NCS)_3]\cdot Me_4Phen\cdot 0.75EtOH$	8/square antiprism	30/32 – Orbach + QTM (2500)	This work

each other, and containing identical donor sites. An example of complex with this type of CE is $(C_5H_5BMe)Er(COT)$ obtained in [37] with the barrier for magnetization reversal in a zero magnetic field of 421 K, which is among the highest values for all Er^{3+}-based SMMs. The similarity of ΔE values for the Er complexes included in Table 3 is attributable to the deviation of the coordination environments from the optimal ones. Due to the small distances between the polyhedron bases, both the double capped trigonal prism and square antiprism significantly differ from a sandwich, which accounts for low barriers for magnetization reversal of Er(III) complexes. This is aggravated by the presence of chemically different donor sites, nitrogen atoms of Me_4Phen and NCS^- and the oxygen atom of water.

For neutral Yb thiocyanate complexes, the barriers for magnetization reversal change slightly on going from the aqua thiocyanate to the Bipy complex, but sharply decrease on going to Phen or Me_4Phen complexes (Table 3). The substantially lower barriers for the complexes with ligands like Phen are caused by greater geometric rigidity of these ligands. According to the Rinehart–Long model, a double capped trigonal prism is a more preferable CP (in comparison with a square antiprism) for increasing the magnetic anisotropy of Yb^{3+}, which is due to the presence of equatorial symmetry elements (caps). However, this trend is unambiguous only for equivalent donor sites in equatorial positions, which compose a uniform ligand field. From this standpoint, small ΔE of $[Yb(Phen)_2(H_2O)(NCS)_3]\cdot Phen\cdot 0.5H_2O$ is attributable to different natures of the caps, that is, the O atoms of water and the N atoms of Phen. The increase in the barrier for magnetization reversal on going from $[Yb(Phen)_2(H_2O)(NCS)_3]\cdot Phen\cdot 0.5H_2O$ to **III** is apparently due to the effect of electron-donating properties of methyl groups, although the contribution of this factor has been adequately studied only for the Dy^{3+}-based SMMs [33]. The ΔE value for complex **III** is rather large both among the Yb thiocyanate complexes and among all Yb-based single-molecule magnets. In addition, the barrier for magnetization reversal for Yb complex **III** is virtually equal to ΔE for the Dy compound **I**, which is a rather rare case for the single-molecule magnets based on lanthanides.

In conclusion, we would like to emphasize several important results of this study. Dy, Er, and Yb thiocyanate complexes containing Me_4Phen retain the trends of formation of complexes with both inner- and outer-sphere ligands [8, 26, 29] and transfer of Me_4Phen from the outer to inner sphere on heating [38], typical of polydentate N-donor ligands. The introduction of the bulky bidentate Me_4Phen ligand into the coordination sphere of the Dy and Yb thiocyanates has an adverse effect on the relaxation characteristics of complexes **I** and **III**. However, the difference between these lanthanides is that in the case of Dy complexes, the introduction of any N-donor ligand results in increasing barrier for magnetization reversal, whereas in the case of Yb compounds, the effect of a ligand such as Bipy is hardly noticeable, unlike the effect of more geometrically rigid ligands. In the case of Er compound **II**, the effect of replacement of water molecule by Me_4Phen is unnoticeable, $\Delta E/k_B$ remaining ~15 K. The effect of coordination of Me_4Phen on the barrier for magnetization reversal is associated with the deviation of the coordination environment from the optimal one for the given complexes.

ACKNOWLEDGMENTS

The study was carried out using research equipment of the Center for Collective Use of Physical Investigation Methods, Kurnakov Institute of General and Inorganic Chemistry, Russian Academy of Sciences.

FUNDING

The synthesis and study of complex **I** were supported by the Russian Science Foundation (grant no. 16-13-10407); the synthesis and study of complexes **II** and **III** were supported by the Russian Foundation for Basic Research (grant no. 18-33-20155). The elemental analysis of the complexes was performed within the state assignment for the Kurnakov Institute of General and Inorganic Chemistry, Russian Academy of Sciences, in the field of fundamental research.

CONFLICT OF INTEREST

The authors declare that they have no conflicts of interest.

SUPPLEMENTARY INFORMATION

The online version contains supplementary material available at https://doi.org/10.1134/S1070328421040060.

REFERENCES

1. Heffeter, P., Jakupec, M.A., Korner, W., et al., *Biochem. Pharmacol.*, 2007, vol. 73, p. 1873.
2. Eliseeva, S.V. and Bünzli, J.-C.G., *Chem. Soc. Rev.*, 2010, vol. 39, p. 189.
3. Stanley, J.M. and Holliday, B.J., *Coord. Chem. Rev.*, 2012, vol. 256, p. 1520.
4. D'Aléo, A., Pointillart, F., Ouahab, L., et al., *Coord. Chem. Rev.*, 2012, vol. 256, p. 1604.
5. Petrosyants, S.P., Dobrokhotova, Zh.V., Ilyukhin, A.B., et al., *Inorg. Chim. Acta*, 2015, vol. 434, p. 160441.
6. Goel, N., *J. Coord. Chem.*, 2015, vol. 68, no. 3, p. 529.
7. Ghose, M., Banerjee, S., Patra, S., and Mukherjea, K.K., *J. Lumin.*, 2016, vol. 180, p. 224.
8. Dobrokhotova, Zh.V., Petrosyants, S.P., Ilyukhin, A.B., et al., *Inorg. Chim. Acta*, 2017, vol. 456, p. 76.

9. Petrosyants, S.P., Ilyukhin, A.B., Gavrikov, A.V., et al., *Inorg. Chim. Acta*, 2019, vol. 486, p. 499.
10. Kot, K., Oczko, G., Puchalska, M., and Starynowicz, P., *Polyhedron*, 2019, vol. 173, p. 114119.
11. Huang, Ch., *Rare Earth Coordination Chemistry: Fundamentals and Applications*, Singapore: Wiley, 2010.
12. Wang, B., Jiang, S., Wang, X., and Gao, S., *Rare Earth Coord. Chem. Fundamentals and Applications*. Pt 9, Huang, Ch.J., Ed., Willey (Asia) Pte Ltd., 2010, p. 355.
13. Guo, F.-S., Day, B.M., Chen, Y.-C., et al., *Science*, 2018, vol. 362, p. 1400.
14. Benelli, C. and Gatteschi, D., *Chem. Rev.*, 2002, vol. 102, p. 2369.
15. Tong, Y.-Z., Gao, C., Wang, Q.-L., et al., *Dalton Trans.*, 2015, vol. 44, p. 9020.
16. Lin, S.-Y., Wang, C., Zhao, L., et al., *Dalton Trans.*, 2015, vol. 44, p. 223.
17. Lannes, A. and Luneau, D., *Inorg. Chem.*, 2015, vol. 54, p. 6736.
18. Pedersen, K.S., Dreiser, J., Weihe, H., et al., *Inorg. Chem.*, 2015, vol. 54, p. 7600.
19. Chen, Y., Ma, F., Chen, X., et al., *Inorg. Chem.*, 2017, vol. 56, p. 13889.
20. Dogaheh, S.G., Khanmohammadi, H., and Sanudo, E.C., *New J. Chem.*, 2017, vol. 41, no. 18, p. 10101.
21. Mandal, L., Biswa, S., Cosquer, G., et al., *Dalton Trans.*, 2018, vol. 47, p. 17493.
22. Pointillart, F., Cador, O., Le Guennic, B., and Ouahab, L., *Coord. Chem. Rev.*, 2017, vol. 346, p. 150.
23. McAdams, S.G., Ariciu, A.-M., Kostopoulos, A.K., et al., *Coord. Chem. Rev.*, 2017, vol. 346, p. 216.
24. Comba, P., Daumann, L.J., Klingeler, R., et al., *Chem. A Eur. J.*, 2018, vol. 24, no. 20, p. 5319.
25. Zhu, Z., Guo, M., Li, X.-L., and Tang, J., *Coord. Chem. Rev.*, 2019, vol. 378, p. 350.
26. Petrosyants, S.P., Dobrokhotova, Zh.V., Ilyukhin, A.B., et al., *Eur. J. Inorg. Chem.*, 2017, p. 3561.
27. Petrosyants, S.P., Babeshkin, K.A., Gavrikov, A.V., et al., *Dalton Trans.*, 2019, vol. 48, p. 12644.
28. TOPAS, Karlsruhe (Germany): Bruker AXS, 2005.
29. Petrosyants, S.P., Ilyukhin, A.B., Dobrokhotova, Zh.V., et al., *Russ. J. Coord. Chem.*, 2017, vol. 43, no. 6, p. 352. https://doi.org/10.1134/S1070328417060057
30. Petrosyants, S.P., Ilyukhin, A.B., Efimov, N.N., and Novotortsev, V.M., *Russ. J. Coord. Chem.*, 2018, vol. 44, no. 11, p. 660. https://doi.org/10.1134/S1070328418110064
31. Kahn, O., *Molecular Magnetism*, New York: VCH, 1993.
32. North, J.M., van de Burgt, L.J., and Dalal, N.S., *Solid State Commun.*, 2002, vol. 123, p. 75.
33. Aravena, D. and Ruiz, E., *Dalton Trans.*, 2020, vol. 49, p. 9916.
34. Chilton, N.F., Collison, D., McInnes, E.J.L., et al., *Nat. Commun.*, 2013, vol. 4, p. 2551.
35. Rinehart, J.D. and Long, J.R., *Chem. Sci.*, 2011, vol. 2, p. 2078.
36. Petrosyants, S.P., Ilyukhin, A.B., Babeshkin, K.A., et al., *Russ. J. Coord. Chem*, 2019, vol. 45, no. 8, p. 592. https://doi.org/10.1134/S1070328419080062

Translated by Z. Svitanko